Density Functional Theoretical Calculations for a Co_2/γ-Al_2O_3 Model Catalyst: Structures of the γ-Al_2O_3 Bulk and Surface and Attachment Sites for Co^{2+} Ions

Toshiaki Taniike,[†] Mizuki Tada,[†] Yoshitada Morikawa,[‡] Takehiko Sasaki,[§] and Yasuhiro Iwasawa*[,†]

Department of Chemistry, Graduate School of Science, The University of Tokyo, Hongo, Bunkyo-ku, Tokyo 113-0033, The Institute of Scientific and Industrial Research, Osaka University, Mihogaoka, Ibaraki, Osaka 567-0047, and Department of Chemistry, Graduate School of Frontier Science, The University of Tokyo, Kashiwanoha, Kashiwa, Chiba 277-8561, Japan

Received: December 16, 2005; In Final Form: January 20, 2006

First-principle density functional theory (DFT) calculations on the electronic state and structure of a $[Co^{2+}]_2/\gamma$-Al_2O_3 model catalyst have been performed in relation to catalysis for unique NO−CO reactions on a Co^{2+} ensemble/γ-Al_2O_3 catalyst. The DFT calculations reveal that a bulk structure of γ-Al_2O_3 is energetically most favorable when aluminum vacancies are evenly dispersed at octahedral sites, and that the (110) plane is exposed as a topmost layer by its neutrality. Two Co^{2+} ions on the (110) surface are supported adjacently to each other in a tetrahedral symmetry. The calculations also demonstrate that the vacant d orbitals of the two Co^{2+} ions are directed toward each other, which brings about an adsorbate−adsorbate interaction between two molecules which adsorb on each of the Co^{2+} ions. This may be an origin of the unique aspect of Co^{2+} ensemble/γ-Al_2O_3 catalysis.

Introduction

Surface catalytic reactions follow the Langmuir−Hinshelwood (LH) or Eley−Rideal (ER) mechanism.[1] LH-type catalytic reactions in the steady state proceed with the aid of adsorption energies of reactants, while a driving force of ER-type catalytic reactions is the collision energies of the reactants. We have found a new reaction phenomenon over a Co^{2+} ensemble/γ-Al_2O_3 catalyst, namely, "surface catalytic NO reactions assisted by gas-phase CO molecules", where the adsorption and reactivity of strongly adsorbed NO molecules are promoted by gas-phase CO molecules that are very weakly adsorbed or undetectable at the catalyst surface.[2−8] The most important issues in this new mechanism are that spectator (or very weakly adsorbed) CO molecules promote the adsorption of NO molecules and open a new reaction pathway. It is still unknown how the spectator CO molecules interact with the catalyst surface and increase the amount and reactivity of adsorbed NO. N_2 and Ar never showed a similar promoting effect, excluding simple contribution of the collision energy to the surface event. Similar catalytic phenomena were observed in the dehydrogenation of ethanol on Nb/SiO_2,[8−10] and water−gas shift reactions on MgO, ZnO, and Rh/CeO_2.[11−14] The discovery of the detail of the mechanism and the origin of the activation and regulation of adsorbed molecules and reaction intermediates may provide a new approach for design of efficient catalysis on surfaces.

The Co^{2+} ensemble/γ-Al_2O_3 catalyst is prepared in a molecularly controlled manner as shown in Figure 1.[6,7,15] The Co^{2+} ions on γ-Al_2O_3 are situated in a trigonally distorted tetrahedral symmetry via Co−O bonds at an average distance of 0.199 nm. The adjacent Co−Co separation is suggested to be about 0.33 nm by EXAFS. NO molecules adsorb as dinitrosyl species on the Co^{2+} ions ($Co(NO)_2$), while CO molecules adsorb very weakly on the catalyst at room temperature and are undetectable at the catalyst surface under the catalytic NO−CO reaction conditions. The spectator CO molecules increase by a factor of 2−3 the amount of dinitrosyl species and remarkably enhance the reaction rate of NO reduction to N_2O. These phenomena are not observed on a Co^{2+}-monomer/γ-Al_2O_3 catalyst though the Co^{2+} monomers on γ-Al_2O_3 have a coordination structure and an oxidation state similar to those of the Co^{2+} ensembles on γ-Al_2O_3.[6] Thus, the new surface phenomenon promoted by gas-phase CO molecules may be due to the existence of another Co^{2+} ion adjacent to a Co^{2+} ion on γ-Al_2O_3. However, it is difficult to find the key issue and detailed mechanism for the

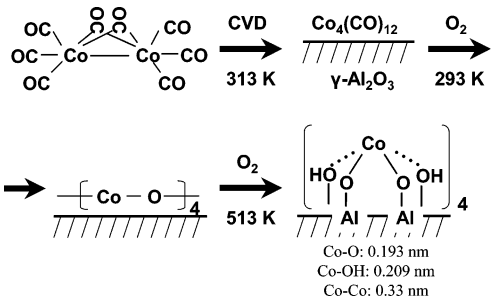

Figure 1. Preparation scheme of the Co^{2+} ensemble/γ-Al_2O_3 catalyst. Attachment of $Co_2(CO)_8$ on a pretreated γ-Al_2O_3 surface by a CVD method leads to formation of $Co_4(CO)_{12}$, which was characterized by FT-IR, EXAFS, diffuse reflectance (DR) UV/vis, and TPD. It is oxidized with O_2 to form a supported $[CoO]_4$ species, which was characterized by EXAFS, DF-UV/vis, and Raman spectroscopy. Finally, by heating the $[CoO]_4/\gamma$-Al_2O_3 at 513 K under vacuum, the $[CoO]_4$ species reacts with surface hydroxyl groups to form the Co^{2+} ensemble/γ-Al_2O_3 catalyst, which was characterized by EXAFS, DR-UV/vis, and Raman spectroscopy.[6,7,15]

* To whom correspondence should be addressed. Phone: +81-3-5841-4363. Fax: +81-3-5800-6892. E-mail: iwasawa@chem.s.u-tokyo.ac.jp.
[†] Graduate School of Science, The University of Tokyo.
[‡] Osaka University.
[§] Graduate School of Frontier Science, The University of Tokyo.

10.1021/jp057341p CCC: $33.50
Published on Web 02/22/2006

surface event assisted by gas-phase molecules experimentally because spectator CO is not spectroscopically detectable at the surface.

The aim of this study is to decide the structure and electronic state of the Co^{2+} ensemble/γ-Al_2O_3 catalyst surface by first-principle density functional theory (DFT) calculations as the first stage of research to explore the surface catalytic NO reduction assisted by gas-phase CO molecules on the surface.

Although γ-Al_2O_3 is one of the most versatile oxide supports,[16] its bulk structure has not been elucidated. It is widely accepted that the γ-Al_2O_3 bulk has a defect−spinel lattice structure with one cation defect per Al_8O_{12} unit to maintain charge balance.[17] There are still debates for the ratio of T_d and O_h sites in the bulk which the cation defects occupy. Transmission electron microscopy (TEM),[18,19] X-ray diffraction (XRD),[20−22] and nuclear magnetic resonance (NMR) studies[23] showed an O_h preference of cation vacancies. On the other hand, electron diffraction,[24,25] XRD,[26] and NMR studies[27−30] gave the opposite preference, T_d vacancies. Various bulk structures have also been proposed by molecular dynamics[31−33] and DFT calculations.[29,34−39] For example, Gutiérrez et al.,[34] Wolverton et al.,[35] and Vijay et al.[36] energetically optimized defect positions in a spinel unit cell and concluded the O_h cation-defect preference as the most stable configuration. On the other hand, Krokidis et al. simulated a dehydration process from boehmite (AlOOH) to γ-Al_2O_3, and obtained a spinel-like structure which had the same T_d Al:O_h Al ratio as that in a defect−spinel structure with all vacancies at T_d sites.[37,38] Sohlberg et al. proposed a different spinel structure involving hydrogen with a HAl_5O_8 composition as a residual of boehmite.[21,39−41] However, Wolverton et al.[35] and Digne et al.[42] claimed that such a H-containing bulk was thermodynamically unstable. Thus, a unified conclusion of the bulk structure of γ-Al_2O_3 has not been obtained yet. Both cluster[43−46] and slab[36,38,47−50] calculations for γ-Al_2O_3 surfaces have been restricted by the unclear bulk structure though numerous experimental studies on the surface characterization of γ-Al_2O_3 [51−69] have been published since the 1950s. Furthermore, to our knowledge, there is only one slab-calculation study about transition-metal adsorption on a γ-Al_2O_3 surface.[70] Thus, this situation has also tempted us to study the γ-Al_2O_3 surface by first-principle DFT calculations.

In the present study we report the structures of the γ-Al_2O_3 bulk and its (110) surface and a model surface structure for the Co_2^{2+} ensemble/γ-Al_2O_3 catalyst which is consistent with the previous experimental results.[2−7,15] The γ-Al_2O_3 bulk has a spinel structure with evenly dispersed O_h vacancies and exposes a relatively neutral (110) plane favorably at the surface. In the model surface structure a Co^{2+} dimer unit is supported on the γ-Al_2O_3(110) plane, where each Co^{2+} ion is situated in a T_d symmetry. We also report that the orientation of vacant orbitals of the two neighboring Co^{2+} ions plays a key role in adsorption and interaction between adsorbed molecules.

Numerical Methods

We performed DFT calculations with the GGA PBE function[71] for the γ-Al_2O_3 bulk and its (110) surface using the program package STATE.[72−80] Vanderbilt-type ultrasoft pseudopotentials[81] and plane waves were employed for a basis set, where the cutoff energy for the wave function was 25 Ry and that for the augmentation charge was 225 Ry. $Al_{16}O_{24}$ was chosen as a unit cell of γ-Al_2O_3, which possessed two cation defects in it. The detail of the unit cell is explained hereinafter. γ-Al_2O_3 surfaces were regarded as a repeated slab model with a vacuum region thicker than 1 nm. The *k*-points for the bulk were $2 \times 4 \times 2$, and those for the surfaces were $2 \times 4 \times 1$. SCF calculations were converged within 5.0×10^{-9} hartree/atom, and the convergence criterion of structure optimization was 1.0×10^{-3} hartree/bohr.

We checked the validity of the above-mentioned parameter set in two steps before extensive calculations for γ-Al_2O_3. In the first step, the lattice constants of an α-Al_2O_3 bulk were optimized in energy. The calculated lattice constants, 0.28060 and 0.44132 nm, were larger than the experimental values by 1.60% and 2.10%, respectively. Considering that GGA functionals often overestimate lattice constants a little,[82−84] the coincidence is sufficiently good. For the second step, the surface reconstruction of an Al-terminated (0001) surface of α-Al_2O_3 was calculated. The employed unit cell was a six-layer $Al_{12}O_{18}$. After structure optimization, the Al atoms in the topmost and the third layer significantly sank down into the bulk direction, and instead the O atoms in the second layer were exposed. Such drastic reconstructions of the Al-terminated (0001) surface were also reported by Manassidis et al.[85] and Wang et al.,[86] and the extent of the reconstructions in their calculations was quite similar to our results. Thus, our parameter set is expected to be sufficiently valid for the γ-Al_2O_3 calculations.

In the calculations for Co^{2+} dimer adsorption, we used DMOL3[87] rather than STATE because an atom-centered basis set becomes much more effective for such systems than a plane-wave basis set. In a typical calculation for a Co_2/Al_2O_3 model, the DMOL3 calculation was ca. 5 times faster than the plane-wave calculation. The exchange-correlation functional was PBE, and the basis set was DNP plus effective core potentials. The *k*-points were $3 \times 4 \times 1$. The convergence criterion for SCF calculations was 1.0×10^{-5} hartree, and those for geometry optimization were 2.0×10^{-5} hartree and 2.1×10^{-3} hartree/bohr. Compatibility between the DMOL3 and plane-wave calculations was ensured by comparison of both the optimized structures of γ-Al_2O_3(110) surfaces and the relative energies of these surfaces calculated by both the programs.

The detailed treatment of the spin states of a Co^{2+} dimer is described below. $Co^{2+}(d^7)$ can have two different spin states: a high spin state (HS) with a spin density of 3 and a low spin state (LS) with a spin density of 1. Therefore, we have considered spin polarization in all calculations including Co^{2+}. The spin-unrestricted calculations were done as follows. At first, an initial spin density (± 3 or ± 1) was assigned to each Co^{2+} ion, and geometry optimization was executed with the amount of total spin fixed at the corresponding value. Next, the electronic wave function of the obtained structure was optimized for the amount of total spin. Finally, the structure was reoptimized without the total spin being fixed. On the basis of this scheme, several different electronic states and structures could be obtained for every Co^{2+} dimer model (they are different from each other in terms of the spin states of the Co^{2+} dimer). Although we compared them in terms of the energies and the structures, only the results for the most stable structure are discussed in this paper.

In our calculations, a weakly interacted Co^{2+} dimer significantly prevented an SCF cycle from converging, because of the multiple d orbitals in a narrow energy region. We cured this problem with a thermal smearing method, which imposes a finite temperature to electronic distribution to improve SCF convergence.[88] A high smearing temperature significantly improves SCF convergence, but worsens the accuracy of the correction term. Therefore, we converged SCF calculations in the following scheme. In the first step, an electronic state was converged with a strong smearing, 0.010 hartree, and then the converged

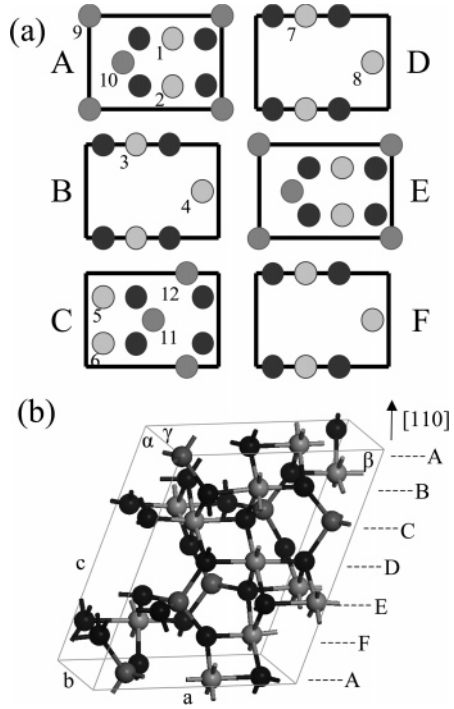

Figure 2. (a) A schematic view of the γ-Al_2O_3 unit cell and (b) its most stable bulk structure. The lattice constants a, b, c, α, β, and γ are 0.79110 nm, 0.55939 nm, 0.96890 nm, 73.260°, 65.940°, and 90.000°, respectively. Key: black balls, O; dark gray balls, T_d Al; gray balls, O_h Al.

electronic state was used as the initial wave function in the next calculation with a milder smearing, 0.008 hartree. In this way, the strength of the thermal smearing was gradually reduced to 0.001 hartree, which was small enough to evaluate accurate energies, structures, and vibrational frequencies.

Results and Discussion

γ-Al_2O_3 Bulk Structure. Figure 2a is a schematic view of the unit cell, $Al_{16}O_{24}$, which includes two cation defects. The size of the unit cell enabled us to evaluate the interaction between cation defects. The unit cell is composed of six layers along a (110) surface (denoted as ABCDEF), and two types of layers align alternately: the dense layers of Al_4O_4 (A, C, E) and the sparse layers of Al_2O_4 (B, D, F). In the dense layers, half of the cation sites have T_d symmetry and the remaining half O_h symmetry, while all cation sites have O_h symmetry in the sparse layers. The lattice constants of the bulk were set to be $a = 0.79110$ nm, $b = 0.55939$ nm, $c = 0.96890$ nm, $\alpha = 73.260°$, $\beta = 65.940°$, and $\gamma = 90.000°$ (see Figure 2b).

For the γ-Al_2O_3 bulk, one must decide which T_d or O_h site the two cation defects occupy and how they interact with each other. In other words, at first the most stable arrangement of the defects has to be decided. Considering the periodic boundary condition, there exist 12 irreducible combinations of the two cation defects: 1−2, 1−3, 1−5, 1−6, 1−7, 3−7, and 3−8 when both the defects occupy O_h sites, 1−9, 3−9, 4−9, 5−9, 7−9, and 8−9 when one defect occupies an O_h site and the other a T_d site, and 9−10, 9−11, and 9−12 when both enter T_d sites. Occupation of nonspinel sites was not considered because of its minority.[17,40] The relative energies of these 12 structures were compared. The results are shown in Figure 3. It was found that an O_h vacancy was favored rather than a T_d vacancy by about 1.1 eV. In addition, the cation defects were repulsive with each other. Indeed, in the most stable arrangements for O_h-O_h, O_h-T_d, and T_d-T_d, the position of one defect was as far away as possible from that of the other in the unit cell. On the basis of these trends, we have decided the most stable bulk structure of γ-Al_2O_3 to be a model of Figure 2b, where the defects occupy 1−7 sites.

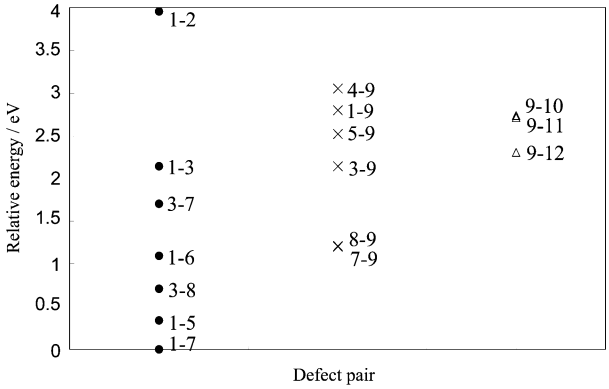

Figure 3. Relative energies for various defect positions. The numbers mean the positions of the cation defects (see also Figure 2a). Key: ●, O_h-O_h; ×, O_h-T_d; △, T_d-T_d.

The trends derived for the defect arrangement agree well with the previous DFT calculations.[34−36] In the previous studies, a defect−spinel lattice was assumed and then the defect arrangement was optimized with energy by DFT calculations at the GGA level. However, there are several spinel-like phases which have different defect structures, δ-, γ-, and θ-Al_2O_3, and vice versa. Among these phases, δ-Al_2O_3 is the most stable, and the energy difference between δ-Al_2O_3 and γ-Al_2O_3 was reported as 0.1 eV per Al_2O_3 unit.[35,89] Therefore, the structure we obtained may be δ-Al_2O_3 rather than γ-Al_2O_3. If we deduce the structure of γ-Al_2O_3 on the basis of Figure 3, candidates for γ-Al_2O_3 are 1−5 and 3−8 (their energies lie in the 0−0.1 eV per Al_2O_3 range). The configurations with any T_d vacancy are out of the energy range in the $Al_{16}O_{24}$ unit cell. However, if one chooses a larger unit cell, the energy cost per Al_2O_3 of the exchange of an O_h vacancy with a T_d vacancy decreases (for example, in the $Al_{16}O_{24}$ unit cell including eight Al_2O_3 units, the formation of one T_d vacancy gives rise to an energy increase of 1.1/8, while it leads to an energy increase of 1.1/16 in an $Al_{32}O_{48}$ unit cell). This means that the formation of a T_d vacancy cannot be completely discarded though the T_d vacancy is minor. Therefore, while we employed the most stable structure of O_h vacancy as the standard one, effects of T_d vacancy were checked when necessary in discussion hereinafter.

γ-Al_2O_3(110) Surface. The next step is to decide the structure of a γ-Al_2O_3 surface. In general, for a spinel bulk the (110) surfaces are preferentially exposed compared with the other low index planes.[51,62] It was reported that the Co^{2+} ensembles on a γ-Al_2O_3 surface showed uniform catalytic activity up to a Co loading of 2 units/nm^2.[6] This result indicates similar structural environments around Co sites, and hence, the major part of a γ-Al_2O_3 surface has the most stable plane because Co^{2+} ions on a mixture of different structural planes with different stabilities never show uniform catalytic activity. Thus, we chose the (110) surface as the support for a Co^{2+} dimer unit. When the bulk (Figure 2b) is cut along the (110) plane, 12 surface structures are obtained. For example, when one inserts a vacuum layer between layer A and layer F, two surface-layer patterns are obtained: ABCDEF and FEDCBA, where the head layer is the surface and the tail layer is on the bulk side. Thus, ABCDEF, AFEDCB, CDEFAB, CBAFED, EFABCD, and EDCBAF are possible patterns when a dense layer is exposed, and FEDCBA, FABCDE, DCBAFE, DEFABC, BAFEDC, and BCDEFA are

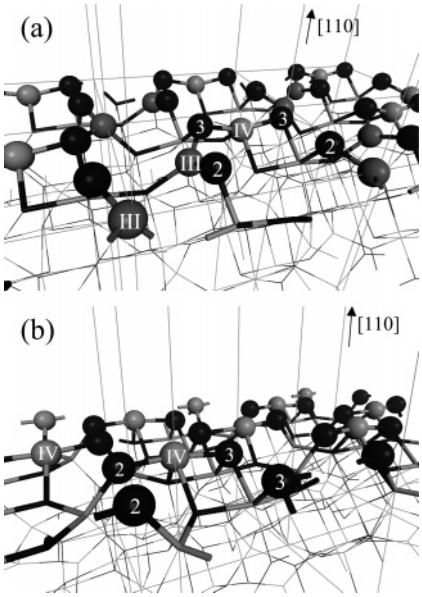

Figure 4. Structures of the clean γ-Al_2O_3(110) surfaces: (a) ABCDEF and (b) FEDCBA. The numbers on the atoms are the coordination numbers of the atoms. The atoms at the topmost layer are drawn by balls and sticks, and those at the subsurface are shown by only sticks. Key:, black balls, O; dark gray balls, T_d Al; gray balls, O_h Al.

possible for the exposure of a sparse layer. Considering that layers C and E and layers B and F are equivalent in terms of layers A and D, the 12 surface patterns reduce to 6: ABCDEF, CDEFAB, CBAFED, FEDCBA, BAFEDC, and DEFABC.

To compare the stability of these six patterns, two sets of calculations were performed: (i) single-point calculations with all atoms fixed at the bulk position and (ii) geometry optimization where only the top four layers were relaxed. The relative energies of ABCDEF, CDEFAB, CBAFED, FEDCBA, BAFEDC, and DEFABC were 0.00, 5.03, 5.60, 0.00, 5.03, and 5.60 eV, respectively, for case i and −2.81, 2.59, 3.36, −2.25, 2.78, and 3.86 eV, respectively, for case ii. The energy difference in case i was due to the different stoichiometries of the layers exposed to the surface, while in case ii the contribution from surface reconstructions was added to the energies of case i. The energy gains by the surface reconstruction given by the absolute value of case ii minus case i varied from 1.74 to 2.81 eV, but it is to be noted that the energy order of the six surfaces is already determined in the calculations of case i. Thus, the main factor to decide the stability of the surfaces is the chemical composition of the exposed layers. For the dense layers, the exposure of layer A (Al_3O_4) was more stable than that of layer C (E) (Al_4O_4) by ca. 5 eV. For the sparse layers, the exposure of layers B and F (Al_2O_4) was more stable than that of layer D (AlO_4) by ca. 1 eV. This trend can be easily explained by the fact that the stable layers have compositions close to Al_2O_3. Concretely, the sums of net charges[51,90] of the topmost layer atoms became closer to 0 in the stable surfaces: +1.50 for ABCDEF, +4.33 for CBAFED, −1.17 for FEDCBA, and −2.67 for DEFABC. We did not compare the energy difference between the dense and sparse layers because the dense and sparse layers were always exposed simultaneously (one type of layer is on the surface side and the other type on the bulk side). Instead, we employed the ABCDEF, FEDCBA, and BAFEDC surfaces to attach a Co^{2+} dimer on them.

Figure 4a is the structure of the ABCDEF surface with the coordination numbers of the surface atoms. One O_h cation defect, two 3-folded T_d Al atoms, one 3-folded O_h Al atom, two 2-folded O atoms, and two 3-folded O atoms are exposed in the unit cell (the coordination number of bulk O is normally 4, and it is 3 when a neighboring cation defect exists). Figure 4b is the surface structure of FEDCBA, where two 4-folded O_h Al atoms, two 2-folded O atoms, and two 3-folded O atoms are exposed. The BACDEF surface has a structure similar to that of the FEDCBA surface except that all the surface O atoms are 2-folded.

We examined the stability of a surface T_d vacancy by replacing a surface O_h vacancy by a surface T_d Al atom on the ABCDEF surface. This exchanged surface is denoted as A′BCDEF. Comparison of the energy of the ABCDEF surface with that of the A′BCDEF surface revealed that the energy difference between a T_d vacancy and an O_h vacancy at the surface became 0.7 eV larger than that for the bulk, i.e., 1.8 eV. The stability of the two surfaces was also compared in terms of the sum of the net charges of the topmost layers. The net charges of layers A and A′ became +1.50 and +0.83, respectively. This analysis was likely to contradict the calculated surface stability at a glance. However, this contradiction was explained by comparing the net charges of each surface atom of layers A and A′. The net charge is a simple estimation of atomic charges.[90] For example, the net charge (Q) of O is defined as $Q = -2 + \sum_i(3/N_i)$, where N_i is the coordination number of the Nth Al atom which is bonded to the O atom. In layer A, the net charges were +0.83 for the two Al(III) atoms, +0.33 for the Al(IV) atom, −0.5 for the two O(II) atoms, and +0.25 for the two O(III) atoms, while in layer A′, the net charges were +1.17 for the Al(III) atom, +0.33 for the two Al(IV) atoms, −0.75 for the two O(II) atoms, and +0.25 for the two O(III) atoms (the Roman numbers in the parentheses show the coordination number). Thus, the Al(III) and the O(II) in layer A′ had net charges which largely deviated from 0 (but they accidentally canceled out). Normally, such highly charged atoms are energetically disadvantageous.[90] Finally, it should be noted that migration of a surface T_d Al atom into an O_h interstice at the subsurface, which was reported in hydrogen-containing γ-Al_2O_3,[48,49] was never detected in both the ABCDEF and A′BCDEF surfaces. Hence, the migration is a specific reconstruction in the hydrogen-containing γ-Al_2O_3.

Co_2/Al_2O_3 Model Catalyst. The attachment of a Co^{2+} dimer on the obtained γ-Al_2O_3 surfaces was examined in the following three cases: (1) reaction of a Co^{2+} dimer with surface hydroxyl groups,[15] (2) replacement of a T_d Al^{3+} ion by $Co^{2+} + H^+$, and (3) replacement of an O_h Al^{3+} ion by $Co^{2+} + H^+$. Several dozens of Co_2/Al_2O_3 models were calculated to obtain the correct one by optimizing structures of the top four layers with the bottom two layers fixed at the bulk positions. Many models were qualitatively very similar, and hence, only representative models and general trends are reported and discussed here. Information about the structure and electronic state of these models is summarized in Table 1.

Co^{2+} Attachment by Reaction with Surface Hydroxyl Groups. Before a Co^{2+} dimer was added onto the surfaces by the attaching reaction, two H_2O molecules per unit cell were dissociatively adsorbed on the clean surfaces. On the ABCDEF surface, the adsorption energy per two H_2O molecules ranged from 1.32 to 4.65 eV depending on the surface sites on which two H^+ and two OH^- ions were bound. In the most stable structure, two H^+ ions adsorbed on the surface O(II) atoms and two OH^- ions adsorbed on the surface Al(III) atom (Figure 5a). Also on the BAFEDC and FEDCBA surfaces, dissociative adsorption of two H_2O molecules occurred,[50] where two H^+ ions adsorbed on the surface O(II) atom and two OH^- ions adsorbed on the surface Al(IV) (see Figure 4b). The largest

TABLE 1: Electronic States and Local Structures of the Co_2/Al_2O_3 Catalyst Models

	Co^{2+} charge[a]	Co^{2+} spin[a]	CN	Co^1–O[b]/nm	Co^2–O[b]/nm	av(Co–O)/nm	Co^1–Co^2 [b]/nm
exptl[6,15]			ca. 4			0.1990	0.33
model 1	0.32, 0.33	1.02, 1.03	4	0.1865, 0.1914, 0.1934, 0.2052	0.1862, 0.1946, 0.1950. 0.2050	0.1947	0.2740
model 2	0.41, 0.38	0.99, 0.64	4	0.1828, 0.1974, 0.1980, 0.1993	0.1854, 0.1855, 0.1863, 0.1998	0.1918	0.4830
model 3	0.57, 0.53	2.69, 2.70	3	0.1902, 0.1904, 0.1918	0.1899, 0.1915, 0.1929	0.1911	0.3164
Co^{2+} monomer[c]	0.58	2.73	3	0.1899, 0.1922, 0.1950		0.1924	

[a] The charge and spin density of Co^{2+} ions are based on the Mulliken analysis. [b] Co^1 and Co^2 represent Co^{2+} ions in Figures 5–7. [c] Monomeric Co/Al_2O_3 model, which is the same as model 3 except that only one surface Al^{3+} is exchanged with $Co^{2+} + H^+$.

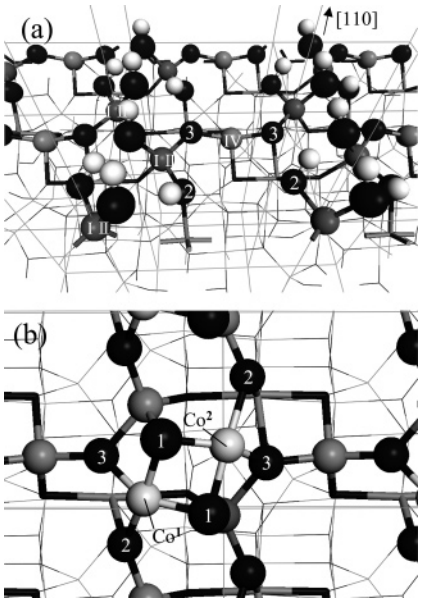

Figure 5. (a) Most stable structure ABCDEF with two H_2O molecules per unit cell surface. (b) Top view of a Co_2/Al_2O_3 model catalyst derived from (a) (model 1). The numbers on the atoms are the coordination numbers of the atoms. Key: black balls, O; dark gray balls, T_d Al; gray balls, O_h Al; light gray balls, Co; white balls, H.

adsorption energies on the BAFEDC and FEDCBA surfaces were 3.47 and 2.87 eV, respectively. For comparison, the same calculations were done on an unstable CBAFED surface. Since there was no O(II) site on the CBAFED surface, two H_2O molecules did not dissociate but molecularly adsorbed on the surface Al(III) site with a 2.15 eV energy gain. This indicates that the exposure of the Al_4O_4 layers remained much more unstable than that of the Al_3O_4 layer after water adsorption.

Next, a Co^{2+} dimer was attached on the hydrated surfaces with removal of four H^+ ions from the surface hydroxyl groups. Figure 5b is a Co_2/Al_2O_3 model made from Figure 5a (model 1). The spin state of the two Co^{2+} ions was low spin (LS), and their spin directions had few effects on the structure and energy of the neighboring Co^{2+} ions. In contrast, a high-spin (HS) electronic state was too unstable to be converged. Each Co^{2+} ion in model 1 is 4-folded by two O(I), O(II), and O(III) atoms (the coordination number of O corresponds to the number of Al atoms bonded to the O atom, and it does not include Co^{2+} ions). The distances of Co–O in model 1 were 0.185–0.205 nm, and the averaged distance was 0.195 nm, which agrees well with the distance determined by EXAFS, 0.199 nm.[6,15] However, the Co–Co distance was 0.274 nm, which is too short compared with the experimental value, 0.33 nm.[6,15] A general trend was found that the O(I) atoms originating from adsorbed water molecules bonded to Co^{2+} strongly to induce a short Co–Co bond or a Co–Al direct bond, both of which were never detected in EXAFS.[6,15] Figure 5b shows an example of a short Co–Co bond. An example of a Co–Al direct bond could be observed when a Co^{2+} dimer was attached on the hydrated FEDCBA surface, replacing four H^+ ions. In this case, as two Co–O(I) bonds were sufficiently far from each other, the distances of the Co–O(I) bonds became less than 0.18 nm, which resulted in the formation of a Co–Al bond instead of a Co–Co bond in model 1.

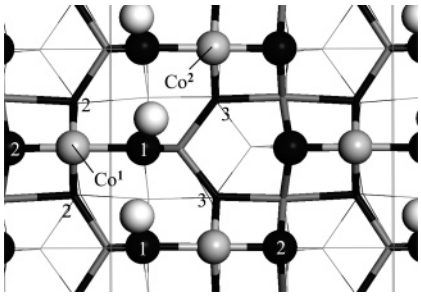

Figure 6. Top view of a $Co_2(O_h)/Al_2O_3$ model catalyst with O_h symmetry (model 2). The numbers on the oxygen atoms are the coordination numbers of the O atoms with respect to Al. Key: black balls, O; gray balls, O_h Al; light gray balls, Co; white balls, H.

These results suggest that isolated hydroxyl groups, O^IH, are not consumed in the attaching reaction. Indeed, when IR spectra for surface hydroxyl groups before and after the Co^{2+} dimer attachment were compared, it was observed that O^IH bands[42,51,54] at 3760–3800 cm^{-1} were unchanged by the Co attachment.[6] On the other hand, bands of $O^{II}H$ and $O^{III}H$ were mainly consumed during the Co attachment. To simulate this experimental result, adsorption of two H_2O molecules per unit cell is not sufficient because it forms only two O^IH and two $O^{II}H$. Adsorption of at least four H_2O molecules per unit cell is needed. However, adsorption of four H_2O molecules in the area of 0.33 nm^2 is not permitted energetically. If one duplicates the $Al_{16}O_{24}$ unit cell in a lateral direction and adds four H_2O molecules on the surface, four O^IH, two $O^{II}H$, and two $O^{III}H$ are formed. Then by exchanging four H^+ ions of the two $O^{II}H$ and two $O^{III}H$ with two Co^{2+} ions, one can obtain a Co_2/Al_2O_3 model catalyst in which each Co^{2+} is 3-folded by O(II), O(III), and O^IH and situated in a T_d symmetry. However, such a duplicating method is quite inefficient compared with the methods described in the next part.

On the basis of the above results and considerations, two alternative attachment methods were employed: (i) replacing a surface Al^{3+} atom by $Co^{2+} + H^+$; (ii) adding a neutral layer including Co^{2+}, Al^{3+}, O^{2-}, and H^+ on the clean surfaces (for example, adding a $2Co^{2+} + 4O^{2-} + 4H^+$ layer on the ABCDEF surface, adding a $2Co^{2+} + Al^{3+} + 4O^{2-} + H^+$ layer on the FEDCBA surface, and so on). In both the methods, models which had any Co–O(I) direct bond were eliminated as candidates. As mentioned above, although Co_2/Al_2O_3 models designed by the two methods amounted to several dozens, these models were qualitatively classified into two types, i.e., $Co_2(O_h)/Al_2O_3$ and $Co_2(T_d)/Al_2O_3$, and only representative models of the two types are reported in the following.

$Co_2(O_h)/Al_2O_3$. Figure 6 represents a model in which the two O_h Al^{3+} ions at the FEDCBA surface are replaced by $2Co^{2+} +$

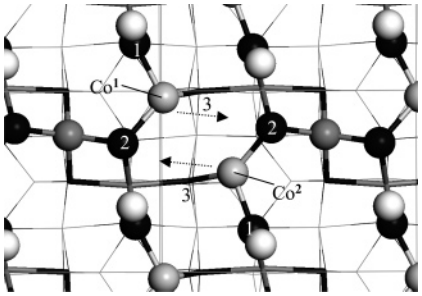

Figure 7. Top view of a $Co_2(T_d)/Al_2O_3$ model catalyst with T_d symmetry (model 3). The description is the same as in Figure 6.

$2H^+$ (model 2). The most stable spin state of the two Co^{2+} ions was LS, and an HS configuration had a 0.33 eV higher energy than that of LS. Generally, in Co^{2+} dimer models with O_h symmetry, Co^{2+} tended to take an LS state since the vicinity around Co^{2+} was sterically crowded with oxygen ligands. In model 2, the spin orientation of the two Co^{2+} ions had negligible effects on their energies due to the large Co−Co distance, 0.483 nm. The two Co^{2+} ions were 4-folded by three O(II) atoms and one O^IH or two O(II) atoms, one O(III) atom, and one O^IH. The Co−O distances were 0.183−0.200 nm, and the averaged Co−O distance, 0.192 nm, agreed with the EXAFS result. However, the Co−Co distance became too large in model 2, and thus, this model showed no dimeric aspects even with adsorbates at the two Co^{2+} ions (described later). Consequently, we have rejected the $Co_2(O_h)/Al_2O_3$ models.

If one replaces the two O_h Al^{3+} ions at the CBAFED surface by $2Co^{2+} + 2H^+$, a Co^{2+} dimer whose Co−Co distance is 0.276 nm is obtained. Such a Co^{2+} dimer strongly adsorbs a CO molecule because of the formation of a Co−CO−Co bridge configuration, but it contradicts the fact that CO is not detectable at the catalyst surface.

$Co_2(T_d)/Al_2O_3$. Figure 7 is the structure of a model in which the two T_d Al^{3+} ions at the ABCDEF surface are replaced by $2Co^{2+} + 2H^+$ (model 3). The spin state of the two Co^{2+} ions was HS, which was more stable than an LS state by 0.73 eV. Again, the spin orientation of the neighboring Co^{2+} gave negligible effects on their energies and structures. Both of the Co^{2+} ions were 3-folded by O(II), O(III), and O^IH. This coordination environment around Co^{2+} is the same as that in the above-mentioned model, which is designed by duplicating the unit cell, then adding four H_2O molecules on the surface, and finally exchanging the surface four H^+ ions by two Co^{2+} ions. The Co−O distances in model 3 were 0.190−0.194 nm, and the averaged Co−O distance, 0.191 nm, did not significantly deviate from the experimental value, 0.199 nm. The deviation is probably due to the lack of one Co−OH interaction, which does not change the qualitative character of the model. The most important point of model 3 is the Co−Co distance of 0.316 nm, which reproduces well the EXAFS value, 0.33 nm. Hence, only the $Co_2(T_d)/Al_2O_3$ model among the three types of Co_2/Al_2O_3 models provides an adequate Co^{2+} dimer. Although a number of similar $Co_2(T_d)/Al_2O_3$ models could be obtained, they were quantitatively very similar and their Co−Co distances ranged from 0.31 to 0.34 nm.

Table 1 shows the electronic states and coordination structures of the Co^{2+} sites for models 1−3. From Table 1, it is found that the 4-folded Co^{2+} ions on the γ-Al_2O_3(110) surfaces always take an LS state and that the LS Co^{2+} ions have a smaller Mulliken charge than the HS Co^{2+} ions, because the covalent nature of the Co−O bonds becomes stronger in an LS state than in an HS state. The order of the strength of the Co−O bonds is Co−O(I) > Co−O(II) > Co−O^IH ≈ Co−O(III), and

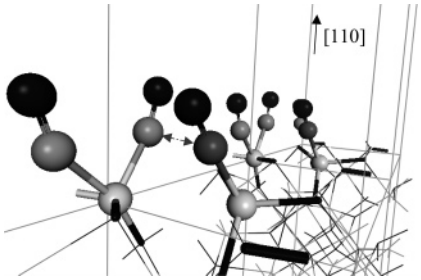

Figure 8. 2NO−CO coadsorption structure in the $Co_2(T_d)/Al_2O_3$ model. The arrow indicates that a NO adsorbate on a Co^{2+} ion is close to a CO adsorbate on the adjacent Co^{2+} ion. Key: black balls, O; light gray balls, Co; dark gray balls, C; gray balls, N.

our calculations for the Co−O distances show Co−O(I) = 0.175−0.183 nm, Co−O(II) = 0.185−0.197 nm, and Co−O^IH or Co−O(III) = 0.192−0.225 nm except in the following two special cases. Model 1 is an example of the special case where Co−O(I)−Co bridge formation weakens the binding ability of O(I) and results in longer Co−O(I) bonds. Another special case is one where Co^{2+} is located immediately above a cation defect. In such a case, the Co^{2+} ion is strongly drawn into the cation defect and the resulting Co−O distances become shorter than the bond distances mentioned above. When the averaged Co−O distances in the three models are compared, one can see that all the models have a similar value, which is slightly shorter than the experimental value. On the other hand, the Co−Co distances in the three models are significantly different from each other, and only model 3 reproduces the experimental Co−Co distance. Our conclusion that Co^{2+} ions occupy the T_d site is also supported by a paper by Moen et al., which reported that reduction of a rhenium-prompted Co_3O_4/γ-Al_2O_3 catalyst yielded Co metal particles and a small fraction of Co^{2+} randomly spread over T_d vacancies of Co_3O_4/γ-Al_2O_3.[91] Note that attachment of Co^{2+} ensembles in the Co_2/γ-Al_2O_3 catalyst led to adjacent Co^{2+} ions in the T_d site rather than randomly dispersed Co^{2+} ions.

Difference between the Co^{2+} Dimer and Co^{2+} Monomer. To examine the difference between the Co^{2+} dimer and Co^{2+} monomer catalysts, additional calculations were conducted for the monomeric Co/Al_2O_3 model in which only one T_d Al^{3+} of the ABCDEF surface was exchanged with $Co^{2+} + H^+$. Results of this monomer model are shown as "Co^{2+} monomer" in Table 1. The monomer model has almost the same feature as that of model 3 for the Co^{2+} dimer, except that electrons are more localized around Co^{2+} in the monomer model. Such a small difference cannot explain the observed large difference between the Co^{2+} monomer and dimer catalysts. Furthermore, the dimer and monomer models had very similar features for NO and CO adsorption (not shown). The fact that the electronic state, local structure, and adsorption property of the Co^{2+} ions are similar between the Co^{2+} monomer and dimer catalysts coincides with the experimental results (UV, XANES, EXAFS, and FT-IR).[6]

Next, we paid attention to unoccupied orbitals of the Co^{2+} dimer in model 3, and found that the unoccupied d orbitals of the two neighboring Co^{2+} ions faced each other. The directions of the unoccupied orbitals are shown as arrows in Figure 7. Therefore, when two molecules simultaneously adsorb on the neighboring two Co^{2+} ions, one adsorbate does interact with the other adsorbate. For example, when two NO molecules adsorb on one Co^{2+} ion in model 3, which is a geminal species, one adsorbed NO is tilted toward the other Co^{2+} (Figure 8). Assuming that the position of Co^{2+} is the same as before adsorption, the angle between the Co−N bond and the surface becomes ca. 55°. Then, when we add a CO molecule on the

adjacent vacant Co^{2+}, the angle between the Co−C bond and the surface also becomes ca. 55° and the CO is tilted toward the Co^{2+} ion coordinated by the geminal NO. Consequently, the NO molecule and the CO molecule approach each other (Figure 8). Considering the bond distances of Co−C and Co−N at 0.18−0.21 nm, the distance between the N atom and the C atom is estimated to be ca. 0.234 nm. This indicates that the two adsorbates should interact with each other because the van der Waals radii of C and N are about 0.15 nm. The adsorbate−adsorbate interaction between the NO and CO molecules never exists on the monomeric Co/Al_2O_3 catalyst. The previous study[15] showed that exposure of the Co^{2+} ensemble/Al_2O_3 catalyst to O_2 led to Co−O−Co bridge formation, while such bridge formation was not observed with the monomeric Co/SiO_2 catalysts. It is suggested in the Co^{2+} ensemble/γ-Al_2O_3 catalyst that both the appropriate distance of Co−Co of about 0.33 nm and the face-to-face orientation of the vacant orbitals yield the interaction between the coadsorbed molecules. We propose that the appropriate separation and orientation of the vacant orbitals of adjacent Co^{2+} ions in a T_d symmetry are the key issues for the new phenomenon of surface catalytic NO−CO reactions assisted by gas-phase CO molecules involving increases in the amount and reactivity of adsorbed NO by CO that is undetectable at the surface of the Co^{2+} ensemble/γ-Al_2O_3 catalyst. The detailed DFT calculations for the CO-promoting effects on them will be reported in the following paper.

Conclusions

To investigate the origin of the new NO−CO phenomenon in the Co_2/γ-Al_2O_3 catalyst, we have performed the following set of density functional theory calculations.

(1) Decision of the γ-Al_2O_3 Bulk Structure. Correlation between the positions of the cation vacancies and the energies of the possible structures was examined, using an $Al_{16}O_{24}$ defect−spinel unit cell including two cation vacancies. An O_h vacancy was more stable than a T_d vacancy by ca. 1.1 eV, and the vacancies were repulsive with each other. The most stable bulk configuration had evenly dispersed O_h vacancies in the bulk.

(2) Decision of the γ-Al_2O_3(110) Surface Structure. Inserting a vacuum layer at various positions of the obtained bulk, the relative energies of six possible (110) surface structures were compared. It was found that the surface stability was mainly determined by the composition of exposed layers rather than the difference in the reconstruction energy of each surface. That is, the exposure of a neutral layer was advantageous, the exposure of an Al_3O_4 layer was more stable than that of an Al_4O_4 layer, and that of an Al_2O_4 layer was more stable than that of an AlO_4 layer. In addition, a surface T_d vacancy destabilized 3-folded surface Al^{3+} and 2-folded surface O^{2-} compared to a surface O_h vacancy.

(3) Attachment of a Co^{2+} Dimer on the γ-Al_2O_3(110) Surface. By adding a Co^{2+} dimer to the obtained (110) surfaces in various ways, we have classified the resulting models into three types and compared them with the experimental results. When a Co^{2+} dimer was attached by a reaction with surface hydroxyl groups, too strong Co−O(I) bonds were always formed, and this resulted in the formation of Co−Co or Co−Al bonds, both of which were never detected by EXAFS. In the case that two Co^{2+} ions were introduced to O_h sites ($Co_2(O_h)/Al_2O_3$), the Co−Co distance became too large and each Co^{2+} behaved as a monomer. On the other hand, only a $Co_2(T_d)/Al_2O_3$ model where two Co^{2+} ions were introduced to T_d sites reproduced all the experimental results. Particularly, the calculated Co−Co distance of 0.316 nm was close to the experimental value. The Co^{2+} dimer behaved like a Co^{2+} monomer in terms of the electronic state and the coordination structure, but the unoccupied orbitals of the neighboring Co^{2+} ions faced each other, resulting in an adsorbate−adsorbate interaction at the neighboring two Co^{2+} ions. The coadsorption of CO and NO on the neighboring Co^{2+} ions and the subsequent interaction between the adsorbates may be the trigger of the new CO-promoting phenomenon in catalytic NO−CO reaction on a Co^{2+} ensemble/γ-Al_2O_3 catalyst.

Acknowledgment. The present study was supported by a Grant-in-aid for The 21st Century COE Program for Frontiers in Fundamental Chemistry from the Ministry of Education, Culture, Sports, Science and Technology. T.T. thanks JSPS for a doctoral fellowship. The calculations were carried out at computer centers of the Tsukuba Advanced Computing Center (TACC), the Institute for Solid State Physics, The University of Tokyo, Kyoto University, Kyushu University, and Nagoya University.

Supporting Information Available: Figure showing the partial densities of states of the two topmost layers for the clean ABCDEF suface and the $Co_2(T_d)/Al_2O_3$ model catalyst. This material is available free of charge via the Internet at http://pubs.acs.org.

References and Notes

(1) Chorkendorff, I.; Niemantsverdriet, W. *Concepts of Modern Catalysis and Kinetics*; Wiley-VCH Verlag: Weinheim, Germany, 2003.
(2) Yamaguchi, A.; Asakura, K.; Iwasawa, Y. *J. Mol. Catal. A* **1999**, *65*, 146.
(3) Kawaguchi, T.; Ichikuni, N.; Yamaguchi, A.; Shido, T.; Onishi, H.; Fukui, K.; Iwasawa, Y. *J. Mol. Catal. A* **1999**, *65*, 146.
(4) Shido, T.; Yamaguchi, A.; Asakura, K.; Iwasawa, Y. *J. Mol. Catal. A* **2000**, *163*, 67.
(5) Yamaguchi, A.; Shido, T.; Asakura, K.; Iwasawa, Y. *Stud. Surf. Sci. Catal.* **2000**, *130*, 605.
(6) Tada, M.; Taniike, T.; Iwasawa, Y. *J. Phys. Chem. B*, to be submitted for publication.
(7) Yamada, M.; Iwasawa, Y. *J. Mol. Catal.* **1984**, *23*, 95.
(8) Iwasawa, Y. *Acc. Chem. Res.* **1997**, *30*, 103.
(9) Nishimura, M.; Asakura, K.; Iwasawa, Y. *J. Chem. Soc., Chem. Commun.* **1986**, 1660.
(10) Nishimura, M.; Asakura, K.; Iwasawa, Y. *Proc.—Int. Congr. Catal., 9th* **1988**, *4*, 1566.
(11) Iwasawa, Y. In *Elementary Reaction Steps in Heterogeneous Catalysis*; Joyner, R. W., van Santen, R. A., Eds.; NATO ASI Series C, Vol. 398, NATO: Brussels, Belgium, 1993; p 287.
(12) Shido, T.; Iwasawa, Y. *J. Catal.* **1990**, *122*, 55.
(13) Shido, T.; Iwasawa, Y. *J. Catal.* **1991**, *129*, 343.
(14) Shido, T.; Iwasawa, Y. *J. Catal.* **1992**, *136*, 493.
(15) Asakura, K.; Iwasawa, Y. *J. Phys. Chem.* **1989**, *93*, 4213.
(16) Oberlander, K. In *Applied Industrial Catalysis*; Leach, B. E., Ed.; Academic Press: New York, 1984.
(17) Zhou, R.-S.; Snyder, R. L. *Acta Crystallogr.* **1991**, *B47*, 617.
(18) Wang, Y. G.; Bronsveld P. M.; DeHosson, J. T. M.; Djuricic, B.; McGarry, D.; Pickering, S. *J. Am. Ceram. Soc.* **1998**, *81*, 1655.
(19) Kryukova, G. N.; Klenov, D. O.; Ivanova, A. S.; Tsybulya, S. V. *J. Eur. Ceram. Soc.* **2000**, *20*, 1187.
(20) Sinha, K. P.; Sinha, A. P. B. *J. Phys. Chem.* **1957**, *61*, 758.
(21) Wang, J. A.; Bokhimi, X.; Morales, A.; Novaro, O.; Lopez, T.; Gomez, R. *J. Phys. Chem. B* **1999**, *103*, 299.
(22) Repelin, Y.; Husson, E. *Mater. Res. Bull.* **1990**, *25*, 611.
(23) Dupree, R.; Lewis, M. H.; Smith, M. E. *Philos. Mag. A* **1986**, *53*, L17.
(24) Saalfed, H.; Mehrotra, B. B. *Ber. Dtsch. Keram. Ges.* **1965**, *42*, 161.
(25) Jayaram, V.; Levi, C. G. *Acta Metall.* **1986**, *37*, 569.
(26) Verwey, E. J. W. *Kristallografiya* **1935**, *91*, 317.
(27) John, C. S.; Alma, N. C. M.; Hays, G. R. *Appl. Catal.* **1983**, *6*, 341.
(28) Chen, F. R.; Davis, J. G.; Fripiat, J. J. *J. Catal.* **1992**, *133*, 263.

(29) Lee, M.-H.; Cheng, C.-F.; Heine, V.; Klinowski, J. *Chem. Phys. Lett.* **1997**, *265*, 673.
(30) Pecharroman, C.; Sobrados, L.; Iglesias, J. E.; Gonzalez-Carreno, T.; Sanz, J. *J. Phys. Chem. B* **1999**, *103*, 6160.
(31) Alvarez, L. J.; Sanz, J. F.; Capitán, M. J.; Odriozola, J. A. *Chem. Phys. Lett.* **1992**, *192*, 463.
(32) Alvarez, L. J.; León, L. E.; Sanz, J. F.; Capitán, M. J.; Odriozola, J. A. *J. Phys. Chem.* **1995**, *99*, 17872.
(33) Mo, S.-D.; Xu, Y.-N.; Ching, W.-Y. *J. Am. Ceram. Soc.* **1997**, *80*, 1193.
(34) Gutiérrez, G.; Taga, A.; Johansson, B. *Phys. Rev. B* **2001**, *65*, 012101.
(35) Wolverton, O.; Hass, K. C. *Phys. Rev. B* **2000**, *63*, 024102.
(36) Vijay, A.; Mills, G.; Metiu, H. *J. Chem. Phys.* **2002**, *117*, 4509.
(37) Krokidis, X.; Raybaud, P.; Gobichon, A.-E.; Rebours, B.; Euzen, P.; Toulhoat, H. *J. Phys. Chem. B* **2001**, *105*, 5121.
(38) Digne, M.; Sautet, P.; Raybaud, P.; Euzen, P.; Toulhoat, H. *J. Catal.* **2004**, *226*, 54.
(39) Sohlberg, K.; Pennycook, S. J.; Pantelides, S. T. *J. Am. Chem. Soc.* **1999**, *121*, 7493.
(40) Ushakov, V. A.; Moroz, E. M. *React. Kinet. Catal. Lett.* **1984**, *24*, 113.
(41) Tsyganenko, A. A.; Smirnov, K. S.; Rzhevskij, A. M.; Mardilovich, P. P. *Mater. Chem. Phys.* **1990**, *26*, 35.
(42) Digne, M.; Sautet, P.; Raybaud, P.; Toulhoat, H.; Artacho, E. *J. Phys. Chem. B* **2002**, *106*, 5155.
(43) De Vito, D. A.; Gilardoni, F.; Kiwi-Minsker, L.; Morgantini, P.-Y.; Porchet, S.; Renken, A.; Weber, J. W. *J. Mol. Struct.: THEOCHEM* **1999**, *469*, 7.
(44) Maresca, O.; Allouche, A.; Aycard, J.-P.; Rajzmann, M.; Clemendot, S.; Hutschka, F. *J. Mol. Struct.: THEOCHEM* **2000**, *505*, 81.
(45) Sanz, J. F.; Rabaâ, H.; Poveda, F. M.; Márquez, A. M.; Calzado, C. J. *Int. J. Quantum Chem.* **1998**, *70*, 359.
(46) Tachikawa, H.; Tsuchida, T. *J. Mol. Catal. A* **1995**, *96*, 277.
(47) Digne, M.; Sautet, P.; Raybaud, P.; Euzen, P.; Toulhoat, H. *J. Catal.* **2002**, *211*, 1.
(48) Sohlberg, K.; Pennycook, S. J.; Pantelides, S. T. *J. Am. Chem. Soc.* **1999**, *121*, 10999.
(49) Sohlberg, K.; Pennycook, S. J.; Pantelides, S. T. *J. Am. Chem. Soc.* **2001**, *123*, 26.
(50) Ionescu, A.; Allouche, A.; Aycard, J.-P.; Rajzmann, M.; Hutschka, F. *J. Phys. Chem. B* **2002**, *106*, 9359.
(51) Knözinger, H.; Ratnasamy, P. *Catal. Rev.—Sci. Eng.* **1978**, *17*, 31.
(52) Tsyganenko, A. A.; Filimonov, V. N. *J. Mol. Struct.* **1973**, *19*, 579.
(53) Nellist, P. D.; Pennycook, S. J. *Science* **1996**, *274*, 413.
(54) Morterra, C.; Ghiotti, G.; Boccuzzi, F.; Coluccia, S. J. *J. Catal.* **1978**, *51*, 299.
(55) Topsøe, N. *J. Catal.* **1980**, *64*, 235.
(56) Beaufils, J.; Barbaux, Y. *J. Chem. Phys.* **1981**, *78*, 347.
(57) Busca, G.; Lorenzelli, V.; Escribano, V. S.; Guidetti, R. *J. Catal.* **1991**, *131*, 167.
(58) Saad, A. B. M.; Ivanov, V. F.; Lavalley, J. C.; Nortier, P.; Luck, F. *Appl. Catal., A* **1993**, *94*, 71.
(59) Coster, D. J.; Blumenfeld, A. L.; Fripiat, J. J. *J. Phys. Chem.* **1994**, *98*, 6201.
(60) Coster, D. J.; Fripiat, J. J.; Muscas, M.; Aroux, A. *Langmuir* **1995**, *11*, 2615.
(61) Morterra, C.; Magnacca, G. *Catal. Today* **1996**, *27*, 497.
(62) Tsyganenko, A. A.; Mardilovich, P. P. *J. Chem. Soc., Faraday Trans.* **1996**, *92*, 4843.
(63) Hendriksen, B. A.; Pearce, D. R.; Rudham, R. *J. Catal.* **1972**, *24*, 82.
(64) Aroux, A.; Muscas, M.; Coster, D. J.; Fripiat, J. J. *Catal. Lett.* **1994**, *28*, 179.
(65) DeCanio, E. C.; Edwards, J. C.; Bruno, J. W. *J. Catal.* **1994**, *148*, 76.
(66) Hietala, J.; Root, A.; Knuuttila, P. *J. Catal.* **1994**, *150*, 46.
(67) Abello, M. C.; Velasco, A. P.; Gorriz, O. F.; Rivarola, J. B. *Appl. Catal., A* **1995**, *129*, 93.
(68) McHale, J. M.; Navrotsky, A.; Perrotta, A. J. *J. Phys. Chem. B* **1997**, *101*, 603.
(69) Zhang, W.; Sun, M.; Prins, R. *J. Phys. Chem. B* **2002**, *106*, 11805.
(70) Rashkeev, S. N.; Sohlberg, K.; Glazoff, M. V., Novak, J.; Pennycook, S. J.; Pantelides, S. T. *Phys. Rev. B* **2003**, *67*, 115414.
(71) Perdew, J. P.; Burke, K.; Ernzerhof, M. *Phys. Rev. Lett.* **1996**, *77*, 3865.
(72) Morikawa, Y. *Phys. Rev. B* **2001**, *63*, 033405.
(73) Morikawa, Y.; Iwata, K.; Terakura, K. *Appl. Surf. Sci.* **2001**, *169*, 11.
(74) Hayashi, T.; Morikawa, Y.; Nozoye, H. *J. Chem. Phys.* **2001**, *144*, 7615.
(75) Morikawa, Y.; Hayashi, T.; Liew, C. C.; Nozoye, H. *Surf. Sci.* **2002**, *507*, 46.
(76) Morikawa, Y.; Liew, C. C.; Nozoye, H. *Surf. Sci.* **2002**, *514*, 389.
(77) Okamoto, Y.; Sugino, O.; Mochizuki, Y.; Ikeshoji, T.; Morikawa, Y. *Chem. Phys. Lett.* **2003**, *377*, 236.
(78) Morikawa, Y.; Ishii, H.; Seki, K. *Phys. Rev. B* **2004**, *69*, 041403.
(79) Okazaki, K.; Morikawa, Y.; Tanaka, S.; Tanaka, K.; Kohyama, M. *Phys. Rev. B* **2004**, *69*, 235404.
(80) Morikawa, Y.; Takahashi, I.; Aizawa, M.; Namai, Y.; Sasaki, T.; Iwasawa, Y. *J. Phys. Chem. B* **2004**, *108*, 14446.
(81) Vanderbilt, D. *Phys. Rev. B* **1991**, *41*, 7892.
(82) Goniakowski, J.; Holender, J. M.; Kantorovich, L. N.; Gillan, M. J. *Phys. Rev. B* **1996**, *53*, 957.
(83) Garcia, A.; Elsässer, J.; Zhu, J.; Louie, S. G.; Cohen, M. L. *Phys. Rev. B* **1992**, *46*, 9829.
(84) Juan, Y. M.; Kaxiras, E. *Phys. Rev. B* **1993**, *48*, 14944.
(85) Manassidis, I.; De Vita, I.; Gillan, M. J. *Surf. Sci. Lett.* **1993**, *285*, L517.
(86) Wang, X.-G.; Chaka, A.; Scheffler, M. *Phys. Rev. Lett.* **2000**, *84*, 3650.
(87) Delley, B. *J. Phys. Chem.* **1990**, *92*, 508.
(88) Weinert, M.; Davenport, J. W. *Phys. Rev. B* **1992**, *45*, 13709.
(89) Yokokawa, T.; Kleppa, O. J. *J. Phys. Chem.* **1964**, *68*, 3246.
(90) Pauling, L. *The Nature of the Chemical Bond*, 3rd ed.; Cornell University Press: Ithaca, NY, 1960.
(91) Moen, A.; Nicholson, D. G.; Rønning, M.; Emerich, H. *J. Mater. Chem.* **1998**, *8*, 2533.